ELSEVIER

Journal of Non-Crystalline Solids 263&264 (2000) 167–179

JOURNAL OF NON-CRYSTALLINE SOLIDS

www.elsevier.com/locate/jnoncrysol

Molecular dynamics simulation of the structure and properties of lithium phosphate glasses

J.-J. Liang [a,*], R.T. Cygan [a], T.M. Alam [b]

[a] *Geochemistry Department, Sandia National Laboratories, Albuquerque, NM 87185, USA*
[b] *Department of Aging and Reliability, Bulk Materials Sandia National Laboratories, Albuquerque, NM 87185, USA*

Abstract

A new forcefield model was developed for the computer simulation of phosphate materials. The model provides a fundamental basis for the evaluation of phosphate glass structure and thermodynamics, and was used to perform molecular dynamics (MD) simulations of a series of lithium phosphate glass compositions ($xLi_2O\cdot(1-x)P_2O_5$, $0\leqslant x\leqslant 0.5$). Microstructural features and thermodynamic properties, as well as their correlations with chemical compositions, were analyzed. An important structural feature observed for the phosphate glasses was the occurrence of ring structures that were related to the chemical composition. Relative stability of the ring structures with respect to the number of phosphate tetrahedra within the ring was investigated using molecular orbital calculations on various phosphate conformations of clusters. An increase in stability was observed as the ring size increases from two- to four-membered rings. A larger abundance of the smallest ring size, the 3-membered rings (P_3O_3), corresponds to the minimum of the glass transition temperature (T_g) in the lithium phosphate glass series (corresponding to the composition $0.2Li_2O\cdot 0.8P_2O_5$). The impact of these strained 3-membered rings, along with the changes in the Li-coordination environment, on determining the spectroscopic and thermodynamic properties of the phosphate glasses is discussed.

1. Introduction

Among the common glass-forming oxides (e.g. SiO_2), phosphorous pentoxide (P_2O_5) and its glass-formation process are the least understood to our knowledge. Yet, phosphate-based materials are important for a variety of applications. The glass-transition temperature (T_g) and thermal-expansion coefficients of phosphate glasses make them candidate materials for glass–metal sealing applications [1], while optical properties such as the rare-earth stimulated-emission cross-sections, thermal-optical coefficients and ultraviolet transparency also make them important for laser glasses [2]. Recent developments of novel compositions for fast-ion conductors [3], as well as uses in biomedical applications [4], have prompted further studies of phosphate glasses.

Knowledge of the structure-property relationships is the key to designing phosphate materials for specific applications. However, in phosphate glasses, these relationships have not received attention because of difficulties in materials preparation. Ultra-phosphate glass compositions, with high P_2O_5 contents (>50% P_2O_5) are hygroscopic, making preparation difficult, as well as presenting

* Corresponding author. Tel.: +1-505 844 9868; fax: +1-505 844 7354.
E-mail address: jliang@sandia.gov (J.-J. Liang).

0022-3093/00/$ - see front matter
PII: S0022-3093(99)00632-8

challenges in measuring properties. Due to these difficulties, a relatively limited number of structural investigations have been reported [5–10], such as X-ray and neutron scattering, Raman and infrared (IR) spectroscopies and solid state nuclear magnetic resonance (NMR) studies. From these investigations, progress has been made in determining short-range and, to some extent, medium-range structures in phosphate glasses. However, a detailed knowledge of certain composition–property relationships is lacking, for example, the non-linear T_g-alkali content relationship experimentally observed in the alkali ultraphosphate solid solution series [7].

Computational approaches have the advantage of bypassing some aspects of the experimental difficulties. In particular, molecular dynamics (MD) simulations can be effectively used to relate physical properties to structural details within the glass. When a proper interatomic interaction model is established, structural information for a given system can be examined in any given scope (e.g. affect of alkali metal or alkali content on T_g). Such effort will build an important bridge between chemical composition, whose properties will be manifested in structural and dynamic properties, and the resultant property variations that are yet to be understood. In this study, the MD simulations for a series of lithium phosphate glasses are presented. Details of the different structural variations as a function of Li_2O concentration are quantified and discussed.

2. Forcefield model

In molecular dynamic simulations, creating a reliable forcefield is the first and most important step in modeling the interatomic interactions that determine the physical properties. In previous MD simulations of metal phosphate glasses [11–13], forcefield models considering primarily two-body interaction models have been used. These models explicitly incorporate electrostatic (Coulombic) and repulsive interactions to describe the chemical bonding between neighboring atoms. They have some success in simulating structures of meta- and pyrophosphate glasses (for the compositions, $M^{n+}_{1/n} \cdot PO_3$ and $M^{n+}_{2/n} \cdot PO_3$, respectively; M is a metal ion of valence $n+$), in which the PO_4 basic building units are much less distorted compared to those in P_2O_5 glass. A potentially useful interaction model has also been proposed in a molecular mechanics simulation of phosphate biominerals [14]. In addition to the two-body interaction terms, three-body interactions involving O–P–O and P–O–P angle-bendings were also included. Structural properties were reproduced reasonably well (within 3% of the experimental values) using this model. However, as this forcefield requires separate parameterizations when oxygen atoms are in different structural environments (terminal or non-bridging vs. bridging), prior knowledge of these different O species is required and the speciation of the O-atom is supposed to be fixed during the simulation process. Such requirement leads to difficulties in MD simulations, particularly at temperatures where bond breaking and bond reforming processes occur.

These difficulties in modeling phosphate chemistry stems from the outer-shell electron configuration of the P atom. Similar to Si, P forms sp^3 hybridization in phosphate compounds [15]. As there are five valence electrons, the tetrahedrally hybridized orbitals are intrinsically anisotropic. This anisotropy is evident in the structure of phosphorous pentaoxide, P_2O_5. Among the four P–O bonds associated with each P atom, three are bridging, $P–O_b$, forming –P–O–P– connectivity, whereas the fourth constitutes the terminal P═O bonds with a π-bond property. While the bond distances [5,6,16–18] for the three $P–O_b$ are similar, between 0.156 and 0.160 nm, those of the P═O bond are from 0.143 to 0.145 nm. These variations in P–O bond lengths are a serious challenge to modeling phosphate material in two aspects. First, a forcefield needs to be constructed such that the asymmetry in the structure can be effectively included in the calculation and second, a mechanism needs to be in place to distinguish the P═O bond from the other $P–O_b$ bonds. This second aspect is especially important with simulations at temperatures at which active bond breaking and reforming will occur.

In the present work, we propose a forcefield model that describes explicit two- and three-body

interactions that is capable of distinguishing P–O_b from P=O bonding while simultaneously treating all the O atoms identically. A Lennard-Jones potential function [19] was used to describe the short-range two-body interactions in addition to the usual Coulombic (electrostatic) interaction. The following form of the Lennard-Jones potential was used:

$$E_{LJ} = D_0\left[\left(\frac{r_0}{r}\right)^{12} - 2\left(\frac{r_0}{r}\right)^{6}\right], \quad (1)$$

in which r represents interatomic distances, r_0 and D_0 are adjustable parameters.

The three-body terms used in the model include O–P–O and P–O–P interactions. The O–P–O term is used to constrain the tetrahedral angles in the PO_4 tetrahedra. It has the form

$$E_{angle} = 1/2k_0(\theta - \theta_0)^2, \quad (2)$$

in which θ is the actual O–P–O angle in the simulated structure, θ_0 is the equilibrium tetrahedral angle of 109.47° and k_0 is a parameter to be determined. The P–O–P term has the same analytical form as Eq. (2) except that the equilibrium angle, θ_0, requires parameterization.

The parameters in Eqs. (1) and (2) were determined by fitting to known crystal structures of P_2O_5. Three different forms of crystalline P_2O_5 are reported [16–18]:

(a) The hexagonal variety (h-P_2O_5). It consists of discrete P_4O_{10} molecules and crystallizes in rhombohedral symmetry. The phase is metastable at room temperature.

(b) The orthorhombic variety with the space group Pnma. It consists of infinite layers built from 3-membered rings of three-corner linked PO_4 tetrahedra. The structure is stable at room temperature.

(c) The orthorhombic variety with the space group Fdd2. It consists of a network of PO_4 tetrahedra linked at three common apices. It is also stable at room temperature.

The two room-temperature stable structures of the P_2O_5 (orthorhombic) crystalline phases were used simultaneously in the parameter fitting processes, using the program GULP [20]. The forcefield parameters were initially fitted using formal charges for each ion. However, while the model reproduced the structures of the crystalline phases, it failed to provide valid thermodynamic parameters, i.e., melting temperatures. It is known that phosphate compounds, as in silicates, have covalent properties [21,22]. Due to this covalent property, the effective ionic charges of the component atoms are reduced. In a forcefield model, the electrostatic interaction is by far the dominant force in holding the atoms together (accounts for over 90% of the total potential energy when formal charges are used to model the phosphate compounds). The use of formal charges will exaggerate the binding or lattice energy of the system and fail to reproduce experimental thermodynamics parameters. One consequence is that glass-transition temperatures and melting temperatures are overestimated in comparison to those observed experimentally [23]. Therefore, to obtain reasonable thermodynamic parameters, such as T_g, it is crucial to use partial charges to describe the Coulombic component of the system energy in the simulations.

Effective ionic charges can be determined experimentally using X-ray diffraction (if the material is crystallized). Alternatively, the charges can be calculated in a first-principle molecular orbital calculation of a cluster representation of the crystalline material. In their Hartree–Fock calculation of the electron structure of the $H_4P_2O_7$ cluster, Uchino and Ogata [21] found that all four O-atoms in a PO_4 tetrahedron (both the individual O-atom bridging or terminal) have a similar effective charge ranging from −0.73 to −0.87. This result provides some support that, ionically, the O-atoms in the PO_4 tetrahedron do not differ. The difference between the bridging and terminal O-atoms is effectively absorbed in the covalent part of the corresponding bonds.

For the P-atom, an effective charge of 1.85 as calculated by Uchino and Ogata was adopted. The partial charge for O-atom was calibrated relative to the effective P charge (maintain electroneutrality for the compound stoichiometry) and found to be −0.74. The O-atom charge corresponds to the smaller margin of the calculated charges for the O-atoms in Uchino and Ogata's work. The partial charge for the Li ion was calculated accordingly to

Table 1
Empirical forcefield parameters[a]

	D_0 (eV)	r_0 (nm)
Two-body interaction		
$P^{1.85}$–$O^{-0.74}$	0.004251	0.21550
$O^{-0.74}$–$O^{-0.74}$	0.012185	0.32743
$Li^{0.37}$–$O^{-0.74}$	0.000668	0.28890
	k_0 (eV/rad^2)	θ_0 (°)
Three-body interaction		
O–P–O	3.5401	109.47
P–O–P	20.9326	135.58

[a] See text for definition of the symbols and parameters.

be 0.37, which is less than the 0.467 given in Uchino and Ogata's work. Forcefield parameters were then readjusted based on the reduced charges. The final fitted parameters are given in Table 1.

A forcefield model and short-range interaction parameters are also needed for the alkali metal. Only two-body interactions between the Li- and the O-atoms are considered, again using the Lennard-Jones potential model. In determining the Li–O interaction parameters, the structure [24] of a crystalline Li–metaphosphate, $LiPO_3$, was used. The resulting Li–O parameters are also included in Table 1.

3. Computational details

3.1. MD simulations

Molecular dynamics simulations were preformed using the Cerius^2 software and the OFF energy program [25]. Six compositions in the solid solution series, $x\mathrm{Li_2O}\cdot(1-x)\mathrm{P_2O_5}$, $x = 0.0$, 0.1, 0.2, 0.3, 0.4 and 0.5, were evaluated. For any given composition in the series, a rectangular simulation box containing a total of 300–400 atoms was generated (Table 2). The experimentally observed density of 2.445 [5] and 2.247 [10] g/cm^3 for P_2O_5 ($x = 0.0$) and $LiPO_3$ ($x = 0.5$), respectively, were used and those for the intermediate compositions were extrapolated between the two end members. Periodic boundary conditions were applied to eliminate edge effects and conserve mass if atoms migrate outside the simulation cell. The atomic positions were randomized and the total energy of the simulation cell was minimized (allowing for geometry reconfiguration) using the forcefield model and parameterization developed in the present work. A molecular dynamics simulation using constant volume and temperature (NVT) canonical ensemble was then performed at 3000 K where active melting was observed for all compositions under study. A thermal bath was used to maintain the temperature of the simulation cell using the Hoover [26] scheme. The Newtonian equation of motion was integrated for every 1 fs time step. A total of 50 000 time steps of integration was used to equilibrate the system, corresponding to a total simulation time of 50 ps. During the simulation, atom connectivities were updated every 10 steps to ensure that active bond breaking and bond reforming processes be allowed while simultaneously two- and three-body interaction energies were calculated for each new configuration. The system was then quenched from 3000 to 300 K in 500 K intervals (the last step from 500 to 300 K). Each step lasted 7 ps, corresponding to a quench rate of $\sim 7.1\times10^{11}$ K/s. Once at 300 K, the system was equilibrated for an additional 50 ps.

Table 2
Number of atoms and cell dimensions of the Li-ultraphosphate glasses, $x\mathrm{Li_2O}\cdot(1-x)\mathrm{P_2O_5}$

x	Number of atoms	Simulation cell dimensions (nm)
0.0	336	$1.68 \times 1.68 \times 1.26$
0.1	396	$2.33 \times 1.56 \times 1.56$
0.2	372	$2.29 \times 1.54 \times 1.54$
0.3	348	$2.27 \times 1.52 \times 1.52$
0.4	324	$2.23 \times 1.49 \times 1.49$
0.5	360	$2.14 \times 1.60 \times 1.60$

3.2. Determination of temperature of glass transition (T_g)

The glass-transition temperature can be determined by monitoring the volume–temperature relationship while keeping the pressure constant. This approach provides a computational analog to the experimental determination of T_g using dilatometry. A similar approach has been used in monitoring the T_g variation in polymers [27]. In the present study, the specific volume–temperature

relationship was examined for the phosphate glass treated as an NPT ensemble (constant pressure and temperature at each given temperature step). A change in slope for the linearly-regressed volume–temperature (V–T) relation corresponds to the glass transition temperature (cf. Fig. 4(a)).

3.3. Ab initio calculation of relative stability of phosphate rings

In support of the MD simulations, the $H_4P_2O_7$ molecular cluster was used to examine electronic structure and obtain the relative energies as a function of the bridging P–O–P bond angle. Hydrogens were used as pseudoatoms allowing the modeling by finite size clusters to represent the extensive crosslinking present in phosphate glasses. For the $H_4P_2O_7$ cluster ab initio molecular orbital calculations were performed at the density-functional-theory (DFT) level using the Gaussian 98 program [28]. The optimization and energy calculations used a 6-311G++(2d,2p) basis set and the B3LYP functionals, which are a linear combination of Becke's three parameter method [29] using the LYP correlational functional of Lee, Yang and Parr [30,31], that include both local and non-local correlations. The geometry of the $H_4P_2O_7$ cluster was optimized in the eclipsed structure and have been described elsewhere [32]. The results of these calculations are similar to those reported by Uchino and Ogata [21].

Ab initio calculations and optimizations of the *n*-membered phosphate rings in various conformations were also obtained using the Gaussian 98 program, but were evaluated at the HF level using the 6-31+G(d) basis set. These additional molecular orbital calculations were initiated to help interpret the relative energies of the rings compared to the ring structures obtained in the MD simulations.

4. Results and discussions

4.1. Phosphorus pentoxide (P_2O_5)

As a test of the robustness of the forcefield model and the corresponding parameterization, the simulation of vitreous P_2O_5 was examined. Under NVT condition at 300 K, the system pressure and the variation over time are examined, while maintaining the density of the glass at the experimentally observed density. The pressure fluctuation over a period of 50 ps was essentially zero (Fig. 1), indicating the ability of the model to reproduce the equilibrium structural state of the system.

The validation of the forcefield model can also be supported by comparing the experimentally observed short-range structure, which is available for P_2O_5 crystals and glass, with those obtained through simulation. The short range P–O distance distribution can be represented using radial distribution function (RDF, represented by $g(r)$ in Fig. 2), which is essentially the probability of finding an atom at a given radial distance from the central atom. For the P_2O_5 crystalline phase that was simulated at 300 K, the RDF for the first coordination sphere of the P–O atom pairs (Fig. 2(a)) shows the distinction between the shorter P═O and the longer P–O_b bonds, in an abundance ratio of 1:3. The bond distance for the P═O bond is 0.141 nm, as compared to the experimentally observed ~0.1448 nm, whereas the average of the P–O_b bonds is 0.155 nm, comparable to the experimentally observed ~0.1575 nm [16–18]. In the quenched P_2O_5 glass, the P–O distance distribution also shows a split (Fig. 2(b)),

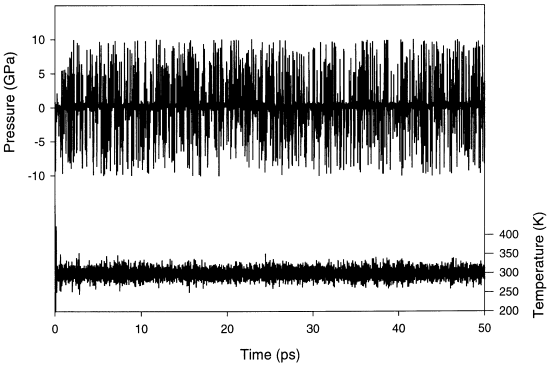

Fig. 1. Dynamic variation of pressure and temperature observed in the MD simulation of P_2O_5 glass ($x = 0.0$) at 300 K under NVT conditions (constant temperature and volume).

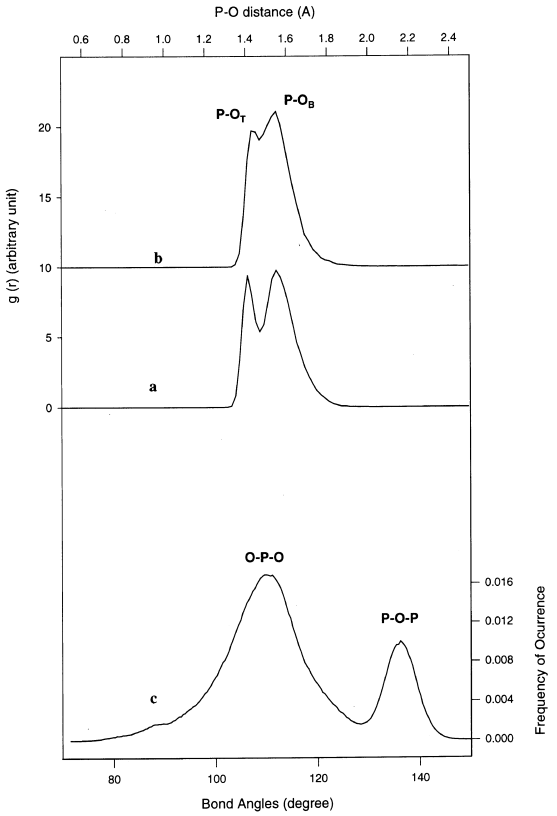

Fig. 2. Interatomic distances and angles simulated for the P_2O_5 crystalline and glass phases. (a) Radial distribution function (RDF, noted as $g(r)$), representing the probability of finding an atom at a given radial distance from the central atom, of the P–O atom pair in the P_2O_5 crystalline phase; (b) RDF of P–O atom pair in the P_2O_5 glass phase; (c) bond angle distribution in the P_2O_5 glass phase.

albeit the difference is less due primarily to the amorphous state of the system and, in part, the relatively large quench rate. The split corresponding to the shorter P═O bond gives an average distance of 0.143 nm and the other split corresponding to the single P–O bonds give an average distance of 0.157 nm. The population ratio is again 1:3. The equivalent P–O distances determined experimentally [6] are 0.1432 ± 0.0005 and 0.1581 ± 0.0003 nm, respectively. The P–O–P angle of the P_2O_5 glass was also modeled well with the forcefield. The experimentally determined [5] P–O–P angle is $137 \pm 3°$, while the simulated being 137° (Fig. 2(c)).

4.2. Short-range structure of the Li-ultraphosphate glass series, $xLi_2O \cdot (1-x)P_2O_5$

Tables 3 and 4 list the mean interatomic distances and angles, respectively, obtained from the equilibrated simulations of the lithium phosphate glass series and Table 5 provides mean coordination numbers for P and Li. Due to the apparent asymmetry and the long trailing tail on the longer distance side in the RDFs of the atom pairs (Fig. 3), distances corresponding to the greatest intensities of the RDF spectra, instead of the averages, are given in the table. The long trailing tail can be effectively suppressed if a smaller quench rate is used in the simulation.

Table 3
Mean interatomic distances (nm) of the Li-ultraphosphate glasses, $x\mathrm{Li_2O} \cdot (1-x)\mathrm{P_2O_5}$

x	⟨P–O⟩	⟨Li–O⟩	⟨O–O⟩	⟨P–P⟩
0.0	0.157		0.249	0.297
0.1	0.155	0.199	0.249	0.291
0.2	0.154	0.197	0.249	0.293
0.3	0.154	0.197	0.249	0.293
0.4	0.154	0.197	0.247	0.295
0.5	0.153	0.197	0.247	0.297

Table 4
Mean angle distribution of the Li-ultraphosphate glasses, $x\mathrm{Li_2O} \cdot (1-x)\mathrm{P_2O_5}$

x	⟨O–P–O⟩	⟨P–O–P⟩
0.0	109	137
0.1	110	137
0.2	110	136
0.3	110	137
0.4	109	137
0.5	110	137

Table 5
Mean coordination number of P and Li of the Li-ultraphosphate glasses, $x\mathrm{Li_2O} \cdot (1-x)\mathrm{P_2O_5}$

x	$N_{\mathrm{P-O}}$	$N_{\mathrm{Li-O}}$
0.0	4.0	
0.1	4.0	4.6
0.2	4.0	4.2
0.3	4.0	4.6
0.4	4.0	4.8
0.5	4.0	5.0

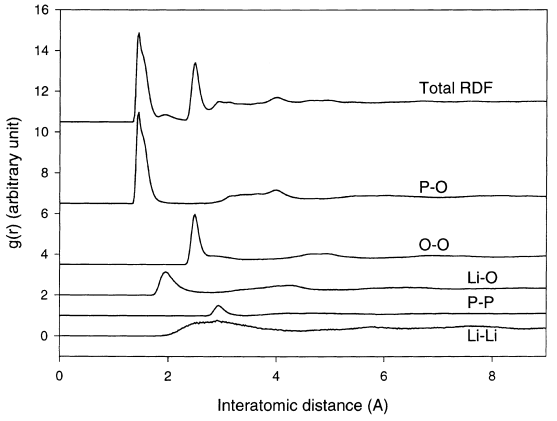

Fig. 3. Radial distribution functions ($g(r)$) for the simulated glass structure of Li-ultraphosphate, $0.2Li_2O \cdot 0.8P_2O_5$.

There is a general trend of decreasing average P–O distance from 0.157 to 0.153 nm as x increases from 0.0 to 0.5 in the solid solution series ($xLi_2O \cdot (1-x)P_2O_5$), while the coordination number of P remains 4.0 throughout the series. The corresponding P–O stretching frequencies are expected to increase as the P–O bond shortens. This increase is consistent with the experimentally observed trend of the major Raman stretching band at $\sim$655 cm^{-1} of the phosphate series [7].

The Li–O and O–O distances remain essentially unchanged as the composition varies. There is a minimum in P–P distance at composition $x = 0.1$ ($0.1Li_2O \cdot 0.9P_2O_5$). The P–P distances increase towards either end-member of the solid solution series. The mean O–P–O and the P–O–P angles also remain apparently invariant, in the range of 109–110° and 136–137°, respectively.

The variation of mean coordination number of the Li ions deserves separate discussion. There is a minimum of $\sim$4.2 corresponding to the composition $x = 0.2$ ($0.2Li_2O \cdot 0.8P_2O_5$). The minimum in the T_g for the lithium phosphate glass series is also observed at this composition. Towards smaller and larger xs, the mean coordination number increases to a maximum of 5.0. The coordination number between 4 and 5 is consistent with recent ^{6}Li NMR investigation of lithium phosphate glasses [33]. While the mean Li–O distances remain constant (Table 3) throughout the series, increasing coordination numbers means an increase in the effective bonding between Li and O atoms. This increase coincides with the increasing T_gs towards both ends of the solid solution series.

4.3. The glass-transition temperatures (T_g)

Fig. 4(a) shows the specific volume–temperature relationship simulated for the P_2O_5 glass as an example in the determination of T_gs for the glass series. A change in slope in the linearly-regressed V–T data from the MD simulations gives a T_g of 628 K. This T_g is close to the experimentally observed 653 K [7]. T_gs for other glass compositions in the series are shown in Fig. 4(b). It can be seen that, although the simulated T_gs are in general less

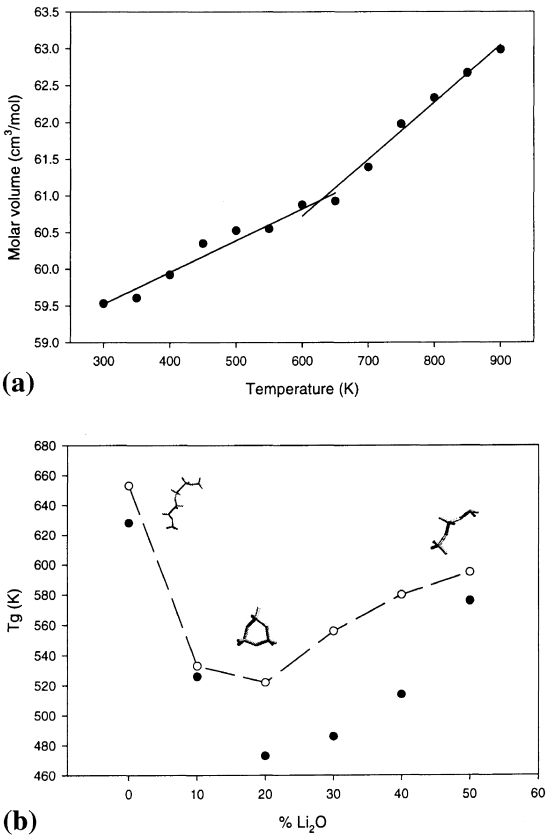

Fig. 4. Glass-transition temperature (T_g) in the lithium phosphate glass, $xLi_2O \cdot (1-x)P_2O_5$ (a) volume–temperature relationship of the simulated P_2O_5 glass and (b) variation of T_g as a function of composition. Solid circle: simulated; open circle: experimentally observed [7].

than the experimentally observed ones, the overall trend of the experimentally observed [7] T_g variation is reproduced. The simulated glass transition temperature at both ends of the solid solution series are relatively high, whereas at ~20% Li_2O, a minimum in T_g is evident.

4.4. Ring structures and their association with T_g

The molecular-level basis for the mechanisms behind the T_g dependence on Li_2O content of the phosphate glasses is puzzling and have been the subject of debate [7–10]. With the MD simulation results, it is possible to examine this dependence using the simulated glass structures, particularly from the medium-range structural point of view. Fig. 5 shows a structural representation of the equilibrated glass for composition $0.2Li_2O \cdot 0.8P_2O_5$. One of the unique structural features of this composition is the formation of 3-membered rings (rings formed by 3 corner-shared PO_4 tetrahedra). In fact, this composition has by far the greatest concentration of 3-membered rings (Fig. 6) observed for any simulated glass. Towards both ends of the compositional series, the abundance of this 3-membered ring decreases and, in the meantime, the abundances of increasingly larger (4-, 5- and 6-membered) rings increases until such a point that chains dominate (Figs. 6 and 7). The highest concentration of the smallest ring size (3-membered rings) coincides with the lowest T_g observed both experimentally and computationally for the composition of $0.2Li_2O \cdot 0.8P_2O_5$.

A recent Raman spectroscopic study [7] of equivalent compositions of phosphate glasses provides experimental evidence that supports the existence of ring-structures in the glass. For compositions with 10–35 mol% Li_2O ($0.10 \leqslant x \leqslant 0.35$), high frequency shoulders were observed on the Raman bands of both the symmetric and asymmetric stretches of non-bridging P–O bonds. It was suggested in the original work [7] that their appearance on the high frequency side of the main stretching bands is due to strained structures. Similar features were found in borate [34] and large-surface-area silicate glasses [35] and were attributed to vibrationally-decoupled three-

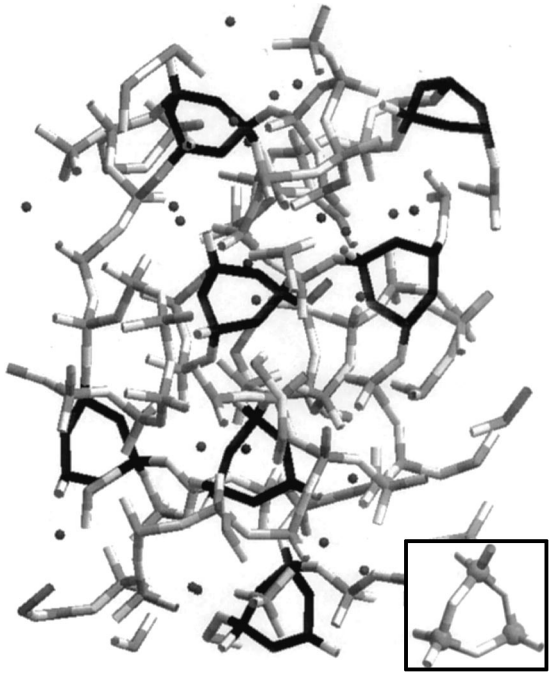

Fig. 5. Simulated structure of phosphate glass composition $0.2Li_2O \cdot 0.8\ P_2O_5$. Note the occurrence of three-membered rings (some of them highlighted in black; see the enlarged representation in the inset). Dark = P; light = O; black dot = Li.

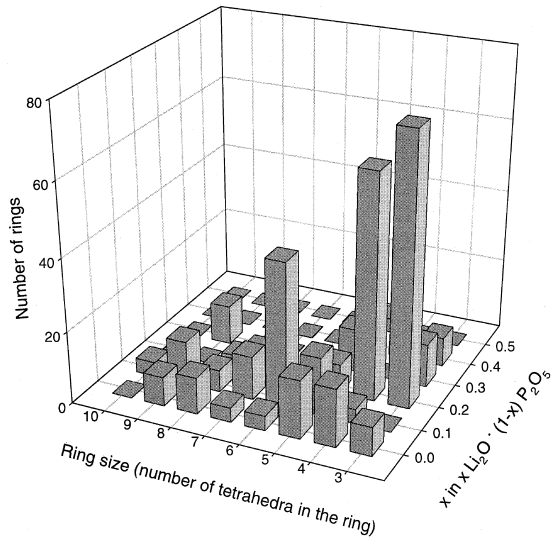

Fig. 6. Distribution of the abundance of various sized rings as a function of composition in the simulated alkali phosphate glass series $xLi_2O \cdot (1-x)P_2O_5$.

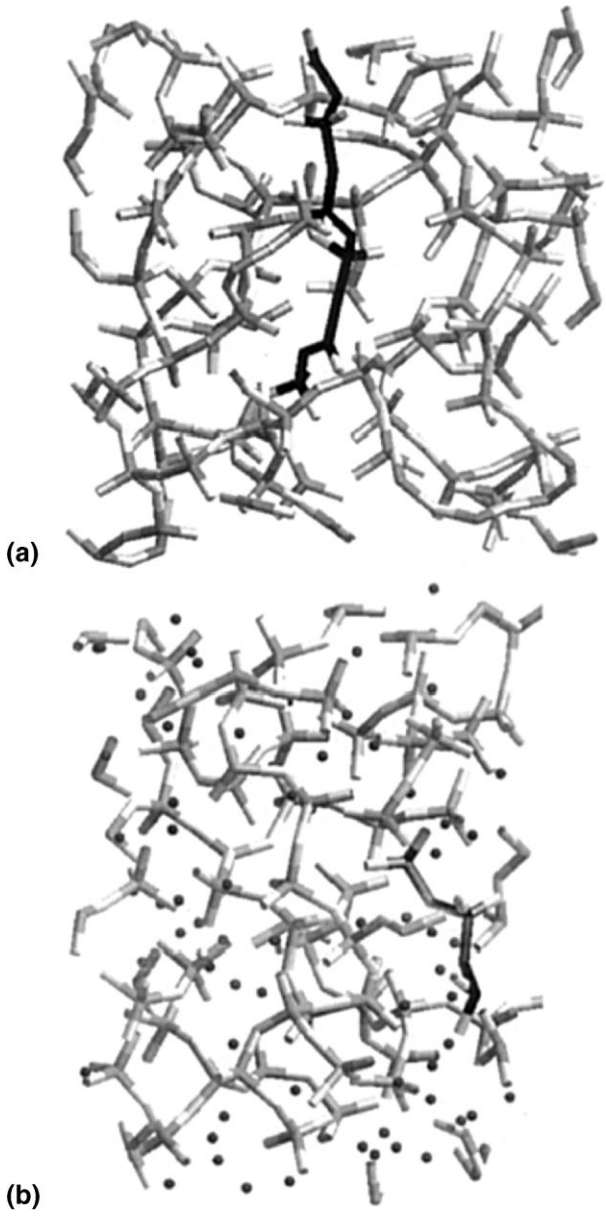

Fig. 7. Simulated glass structures of the end-member compositions of the alkali phosphate glass, $x\mathrm{Li_2O}\cdot(1-x)\mathrm{P_2O_5}$ (a) $x=0.0$; (b) $x=0.5$. Dark = P; light = O; black dot = Li. Notice the dominance of chains in the structure (one of the chains being highlighted in green in each picture).

and four-member tetrahedral rings using ab initio calculation [36]. Relative stability of different ring configurations in silicate glasses was recently examined using molecular orbital calculations [37]. The heats of formation were found to become more negative (towards more stable configurations) as ring size grows from two- to six-members.

We observed similar ring strain effects in our phosphate glass based on the ab initio calculations on n-membered phosphate rings. In contrast to the simple ring structures in silicate rings, the presence of the terminal oxygen on the phosphate gives rise to numerous conformations for each ring size. Fig. 8 shows the HF 6-31 G(d) optimized conformations for the $n = 2$-, 3- and 4-membered phosphate rings. The structural parameters and associated energies for these different confirmations are given in Table 6. As a first approximation of the relative stability of these ring systems, one can follow an approach similar to that presented by Galeener et al. [35] for silicate ring systems, where the internal P–O–P bond angle is used to estimate relative energies. In Fig. 9 the energy as a function of the P–O–P bond angle in the $H_4P_2O_7$ cluster is shown. A minimum in energy is observed for a P–O–P bond angle of 138°. Different P–O–P angles observed in the 2-, 3- and 4-membered rings are also shown, with the relative energy per P–O–P angle being given in Table 6. The energy associated with the 2-membered rings is $\sim$46 kcal mol^{-1}, supporting the failure to observe these rings in the MD simulations. The most stable form of the 3-membered ring (partial cone, pc) has an internal P–O–P angle of 122° within the ring that is $\sim$3.6 kcal mol^{-1} higher in energy than the optimal P–O–P bond angle. As n increases the P–O–P bond angle tends toward or is near the optimal 138°. These results tend to support the idea that the 3-membered ring is less stable with respect to $n \geqslant 4$-sized rings. Therefore, the glass composition that has the most abundant small rings is the least thermodynamically stable and gives the lowest T_g. This composition corresponds to $0.2Li_2O \cdot 0.8P_2O_5$, whose glass structure has the largest abundance of 3-membered ring, the smallest ring unit observed in the glass. As the abundance of the small rings decrease and those of the larger rings increase (Fig. 6), the energetic stability of the glasses increases and so does the associated T_g. The dominance of chains, that can be viewed as rings with infinite number of members, at both ends of the solid solution series (Fig. 7) marks the peak of energetic stability and the associated T_g.

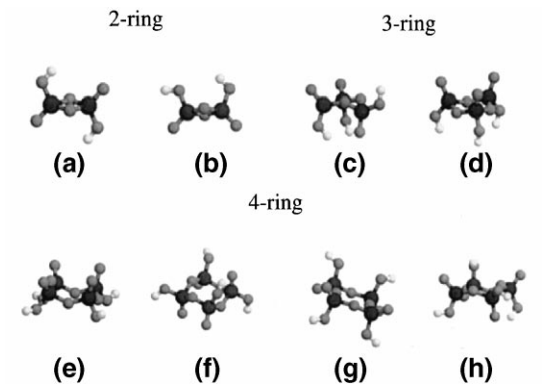

Fig. 8. Representations of the optimized structures for 2-membered phosphate rings (a) *trans*; (b) *cis*; 3-membered phosphate rings; (c) partial cone (pc); (d) cone (c), four-membered phosphate rings; (e) cone (c); (f) partial cone (pc); (g) 1, 2 alternate (1, 2 alt) and (f) 1, 3 alternate (1, 3 alt).

One point of concern is the fact that the calculated thermodynamic properties (such as T_g) and microstructure (such as ring-size) in the simulated glasses are a function of cooling rate during MD simulation [38]. However, as the cooling rate used is identical for each composition in the Li-phosphate series, we still have a valid base for comparison. While the absolute numbers for the thermodynamic and structural parameters (such as T_g and percentages of different ring size) may not be compared directly to experiment due to the quench rate used in the simulation, the relative trends in parameter variation are consistent. Another important property that also varies as a function of composition, the density, can be analyzed similarly. It will be the focus of further investigation.

The discovery that the decreasing concentration of ring structures, to produce long phosphate chains, correlates with increasing T_g (Figs. 4(b) and 7) and provides insight into a principal structural control of T_g variation. These MD simulations support the postulate that the increase in T_g beyond 20 mol% Li_2O is controlled by the increasingly important interaction of the long phosphate chains in the glass structure [39]. The concept of 'repolymerization' of the phosphate network via O–Li–O linkages have also been forwarded as another structural factor that may affect T_g variation [40]. A more detailed analysis of the Li coordination environment is underway.

Table 6
Optimized structural parameters and associated energies for *n*-membered phosphate rings clusters calculated at the HF/6-31+G(d) level.

Structure[a]	Bond angles (°)		Bond distances P–O (Å)[b]	ΔE_{HF} (kcal mol^{-1})[c]	ΔE_{angle} (kcal mol^{-1})[d]
	P–O–P[e]	O–P–O[e]			
	2-Ring				
Cis	94.7	85.3	1.622	–	46.9
Trans	94.8	85.2	1.625	0.54	46.6
3-Ring					
Partial cone	140.0	99.6	1.590	–	~0
	122.0	107.3	1.600		3.6
			1.620		
Cone	129.8	99.0	1.607	11.4	0.7
4-Ring					
1, 3 alternate	132.1	100.0	1.577	–	0.3
	133.8	100.5	1.582		0.1
	134.9	102.1	1.584		~0
	138.6	102.9	1.585		~0
			1.589		
			1.594		
			1.621		
			1.625		
Partial cone	131.9	100.0	1.584	1.6	0.3
	133.3	100.7	1.585		0.1
	136.4	102.1	1.586		~0
	136.8	102.4	1.588		~0
			1.598		
			1.600		
			1.604		
			1.616		
Cone	134.5	100.4	1.590 (4×)	7.6	0.2
	137.6 (2×)	100.4	1.588 (2×)		~0
	141.3	101.8	1.592 (2×)		~0
		101.8			
1, 2 alternate	140.0 (2×)	100.6 (4×)	1.569 (4×)	10.0	~0
	167.8 (2×)		1.586 (4×)		3.4

[a] Optimized structural conformations are shown in Fig. 8.
[b] Only bridging inner-ring P–O bond distances are shown.
[c] Relative HF energy differences for same sized phosphate rings.
[d] Relative energy for P–O–P bond angles based on the linear dimer P–O–P energy relationship shown in Fig. 9.
[e] Only inner-ring P–O–P and O–P–O angles are shown.

4.5. The effect of quench rate on the simulated Q^n species distribution

The degree of polymerization in a phosphate system can be described by the Q^n notation, where $0 \leqslant n \leqslant 4$ and represents the number of bridging oxygens on a PO_4 tetrahedron. Only Q^n species of $0 \leqslant n \leqslant 3$ were observed in phosphate crystals and glasses (cf. [7]). The degree of polymerization, or the relative population of the Q^n species, is composition dependent. Vitreous P_2O_5 and polymorphs of crystalline equivalents have the largest observed degree of polymerization, with 100% Q^3 in the structure [5,6,16–18]. With increasing alkali (Li) content, the phosphate is increasingly depolymerized [7–9] with an observed increase in the proportions of Q^2 and Q^1. Table 7 shows the relative population of the Q^n species in the simulated

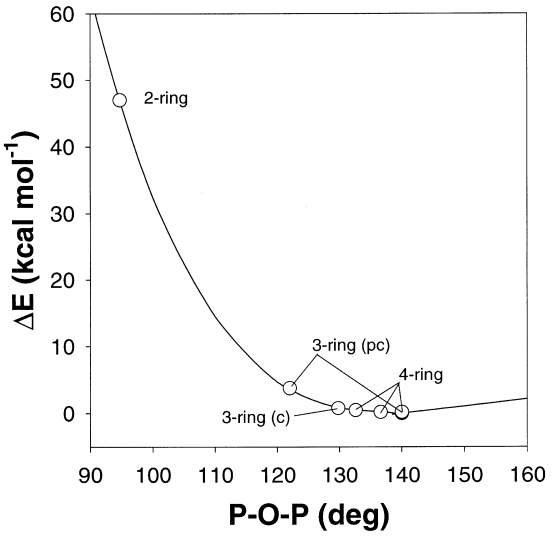

Fig. 9. Energy from Hartree–Fock calculations as a function of bridging P–O–P bond angle in the $H_4P_2O_7$ cluster. The P–O–P bond angle for the different *n*-membered phosphate rings are shown for comparison.

Table 7
Relative populations (%) of Q^n species in the Li-ultraphosphate glasses, $xLi_2O \cdot (1-x)P_2O_5$

x	Q^0	Q^1	Q^2	Q^3	Q^4
0.0		9	31	47	13
				100[a]	
0.1		2	31	52	15
			11[a]	89[a]	
0.2	1	13	23	50	13
			25[a]	75[a]	
0.3		6	39	54	1
			43[a]	57[a]	
0.4		14	43	42	1
			67[a]	33[a]	
0.5	1	24	54	21	
			100[a]		

[a] Ideal Q^n-distribution calculated based on equations [7], $f_{Q^2} = x/(1-x)$ and $f_{Q^3} = (1-x/(1-x))$.

glasses as compared to the ideal numbers [7]. The relative dominance of the Q-species was reproduced as the ideal, although there is a larger spread in the Q-distributions. The depolymerization effect of alkali (Li) addition is also evident in the results. The spread of Q-distribution, particularly the presence of Q^4 species for compositions of $0.0 \leqslant x \leqslant 0.2$, is probably related to the quench rate used in the simulation. Indeed, when the quench rate is decreased from the usual rate of 7.1×10^{11} K/s to 4.0×10^{11} K/s and then to 2.0×10^{10} K/s, the proportion of Q^3 for the P_2O_5 glass ($x = 0.0$, 100% experimentally) increased from 47% to 55% and then to 60%, respectively. Yet, the quench rate in the experimental preparation of the glass [5,6] is in the order of degrees per second, which is far beyond the ability of current computing resources.

5. Conclusions

The molecular dynamics simulations based on the developed phosphate forcefield provide an atomic-based model for the interpretation of the structure and thermodynamic properties of phosphate glasses. The ability to obtain equilibrated glass structures and monitor their dilatancy at constant pressure provides a method for the determination of glass formation temperatures. Ring structures were observed in the alkali phosphate glasses and were closely related to the chemical composition. The highest abundance of smallest ring size (3-membered ring) that is energetically least favorable (as based on ab initio calculations of cluster molecules) corresponds to the minimum of T_g in the phosphate glass series. This structural feature, along with variations in the Li coordination environment, may determine the spectroscopic and thermodynamic properties observed in the phosphate glass. These newly developed simulation methods will prove invaluable for future evaluation of structure–property relations and, ultimately, the design of new phosphate-based materials.

Acknowledgements

The authors acknowledge the support of the US Department of Energy, Office of Basic Energy Sciences, Materials Science Research. Richard Brow provided invaluable support and guidance during the early stages of this project. The comments of an anonymous reviewer helped to improve the clarity of the manuscript. Sandia is a multiprogram Laboratory operated by Sandia Corporation, a Lockheed Martin Company, for

the United States Department of Energy under the contract DE-AC04-94AL85000.

References

[1] J.A. Wilder, J. Non-Cryst. Solids 38&39 (1980) 879.
[2] M.J. Weber, J. Non-Cryst. Solids 123 (1990) 208.
[3] K. Kawamura, H. Hosono, H. Kawazoe, N. Matsunami, Y. Abe, J. Ceram. Soc. 104 (1996) 688.
[4] R.B. Heimann, T.A. Vu, M.L. Wayman, Euro. J. Mineral. 9 (1997) 597.
[5] U. Hoppe, G. Walter, R. Kranold, D. Stachel, Z. Natur. A 53 (1998) 93.
[6] U. Hoppe, G. Walter, A. Barz, D. Stachel, A.C. Hannon, J. Phys.: Condens. Matter 10 (1998) 261.
[7] J.J. Hudgens, R.K. Brow, D.R. Tallant, S.W. Martin, J. Non-Cryst. Solids 223 (1998) 21.
[8] J. Swenson, A. Matic, A. Brodin, L. Borjesson, W.S. Howells, Phys. Rev. B 58 (1998) 11331.
[9] T.M. Alam, R.K. Brow, J. Non-Cryst. Solids 223 (1998) 1.
[10] K. Muruganandam, M. Seshasayee, S. Patnaik, Solid State Ionics 89 (1996) 313.
[11] G. Cormier, J.A. Capobianco, A. Monteil, J. Non-Cryst. Solids 168 (1994) 115.
[12] G. Cormier, J.A. Capobianco, C.A. Morrison, J. Chem. Soc. Faraday Trans. 90 (1994) 755.
[13] G.G. Boiko, N.S. Andreev, A.V. Parkachev, J. Non-Cryst. Solids 238 (1998) 175.
[14] M.G. Taylor, K. Simkiss, M. Leslie, J. Chem. Soc. Faraday Trans. 90 (1994) 641.
[15] F.L. Galeener, J.C. Mikkelsen, Solid State Commun. 30 (1979) 505.
[16] El.H. Arbib, B. Elouadi, J. Solid State Chem. 127 (1996) 350.
[17] D. Stachel, I. Svoboda, H. Fuess, Acta Crystallogr. C 51 (1995) 1049.
[18] M. Jansen, B. Luer, Z. Kristallogr. 177 (1986) 149.
[19] J.E. Lennard-Jones, Proc. Roy. Soc. London A 106 (1924) 441.
[20] J.D. Gale, General Utility Lattice Program developed at the Royal Institution of Great Britain/Imperial College 1992–1994.
[21] T. Uchino, Y. Ogata, J. Non-Cryst. Solids 181 (1995) 175.
[22] P.C. Harkins, G. Petersson, P. Haake, J. Inorg. Biochem. 61 (1996) 25.
[23] B. Vessal, M. Amini, D. Fincham, C.R.A. Catlow, Philos. Mag. B 60 (1989) 753.
[24] J.C. Par, I. Tordjman, Acta. Crystallogr. B 32 (1976) 2960.
[25] The MD simulations were preformed using the Cerius^2 software package and the off energy program, Molecular Simulations Inc.
[26] W.G. Hoover, Phys. Rev. A 31 (1985) 1695.
[27] R.J. Roe, Adv. Polymer. Sci 116 (1994) 111.
[28] M.J. Frisch, G.W. Trucks, H.B. Schlegel, G.E. Scuseria, M.A. Robb, J.R. Cheeseman, V.G. Zakrzewski, J.A. Montgomery Jr., R.E. Stratmann, J.C. Burant, S. Dapprich, J.M. Millam, A.D. Daniels, K.N. Kudin, M.C. Strain, O. Farkas, J. Tomasi, V. Barone, M. Cossi, R. Cammi, B. Mennucci, C. Pomelli, C. Adamo, S. Clifford, J. Ochterski, G.A. Petersson, P.Y. Ayala, Q. Cui, K. Morokuma, D.K. Malick, A.D. Rabuck, K. Raghavachari, J.B. Foresman, J. Cioslowski, J.V. Ortiz, B.B. Stefanov, G. Liu, A. Liashenko, P. Piskorz, I. Komaromi, R. Gomperts, R.L. Martin, D.J. Fox, T. Keith, M.A. Al-Laham, C.Y. Peng, A. Nanayakkara, C. Gonzalez, M. Challacombe, P.M.W. Gill, B. Johnson, W. Chen, M.W. Wong, J.L. Andres, C. Gonzalez, M. Head-Gordon, E.S. Replogle, J.A. Pople, Gaussian 98, Revision A.6, Gaussian, Inc., Pittsburgh, PA, 1998.
[29] A.D. Becke, Phys. Rev. A 38 (1988) 3098.
[30] C. Lee, W. Yang, R.G. Parr, Phys. Rev. B 37 (1988) 785.
[31] B. Miehlick, A. Savin, H. Stoll, H. Preuss, Chem. Phys. Lett. 157 (1989) 200.
[32] T.M. Alam, in: J.C. Facelli, A.C. de Dios (Eds.), Modelling NMR Chemical Shifts Gaining Insight into Structure and Environment, ACS Symposium Series #732, American Chemical Society, Washington, DC, 1999, ch. 22, p. 320.
[33] T.M. Alam, S. Conzone, R.K. Brow, T.J. Boyle, J. Non-Cryst. Solids 258 (1999) 140.
[34] A.K. Hassan, L.M. Torell, L. Borjesson, H. Doweidar, Phys. Rev. B 45 (1992) 12797.
[35] F.L. Galeener, R.A. Barrio, E. Martinez, R.J. Elliott, Phys. Rev. Lett. 53 (1984) 2429.
[36] T. Uchino, Y. Tokuda, T. Yoko, Phys. Rev. B 58 (1998) 5322.
[37] L.L. Hench, J.K. West, Annual Rev. of Mater. Sci. 25 (1995) 37.
[38] K. Vollmayr, W. Kob, K. Binder, Phys. Rev. B 54 (1996) 15808.
[39] J.J. Hudgens, S.W. Martin, J. Am. Ceram. Soc. 76 (1993) 1691.
[40] U. Hoppe, J. Non-Cryst. Solids 195 (1996) 138.